

The **UT \bar{f}** Collaboration Report on the Status of the Unitarity Triangle beyond the Standard Model

I. Model-independent Analysis and Minimal Flavour Violation



UT \bar{f} Collaboration :

M. Bona^(a), **M. Ciuchini**^(b), **E. Franco**^(c), **V. Lubicz**^(b),
G. Martinelli^(c), **F. Parodi**^(d), **M. Pierini**^(e), **P. Roudeau**^(f),
C. Schiavi^(d), **L. Silvestrini**^(c), **A. Stocchi**^(f), and **V. Vagnoni**^(g)

^(a) INFN, Sez. di Torino,
Via P. Giuria 1, I-10125 Torino, Italy

^(b) Dip. di Fisica, Università di Roma Tre and INFN, Sez. di Roma III,
Via della Vasca Navale 84, I-00146 Roma, Italy

^(c) Dip. di Fisica, Università di Roma “La Sapienza” and INFN, Sez. di Roma,
Piazzale A. Moro 2, I-00185 Roma, Italy

^(d) Dip. di Fisica, Università di Genova and INFN,
Via Dodecaneso 33, I-16146 Genova, Italy

^(e) Department of Physics, University of Wisconsin,
Madison, WI 53706, USA

^(f) Laboratoire de l’Accélérateur Linéaire,
IN2P3-CNRS et Université de Paris-Sud, BP 34, F-91898 Orsay Cedex

^(g)INFN, Sez. di Bologna,
Via Irnerio 46, I-40126 Bologna, Italy

Abstract

Starting from a (new physics independent) tree level determination of $\bar{\rho}$ and $\bar{\eta}$, we perform the Unitarity Triangle analysis in general extensions of the Standard Model with arbitrary new physics contributions to loop-mediated processes. Using a simple parameterization, we determine the allowed ranges of non-standard contributions to $|\Delta F| = 2$ processes. Remarkably, the recent measurements from B factories allow us to determine with good precision the shape of the Unitarity Triangle even in the presence of new physics, and to derive stringent constraints on non-standard contributions to $|\Delta F| = 2$ processes. Since the present experimental constraints flavour models with Minimal Flavour Violation, we present the determination of the Universal Unitarity Triangle that can be defined in this class of extensions of the Standard Model. Finally, we perform a combined fit of the Unitarity Triangle and of new physics contributions in Minimal Flavour Violation, reaching a sensitivity to a new physics scale of about 5 TeV. We also extrapolate all these analyses into a “year 2010” scenario for experimental and theoretical inputs in the flavour sector. All the results presented in this paper are also available at the URL <http://www.utfit.org>, where they are continuously updated.

1 Introduction

With the increasing precision of the experimental results, the Unitarity Triangle (UT) analysis shows the impressive success of the CKM picture in describing CP violation in the Standard Model (SM). UT parameters have been consistently determined using both CP-conserving ($|V_{ub}/V_{cb}|$, Δm_d and $\Delta m_d/\Delta m_s$) and CP-violating (ε_K and $\sin 2\beta$) processes [1]. Additional measurements of several combinations of angles of the UT, especially γ from $B \rightarrow DK$ and α from charmless B decays, confirm this picture [1].

This success becomes a puzzle once, as a possible solution to the gauge hierarchy problem, the SM is considered as an effective theory valid up to energies not much higher than the electroweak scale. Indeed, even in the favourable case in which the theory above the cutoff is weakly coupled, such as the Minimal Supersymmetric Standard Model, large contributions to Flavour Changing Neutral Current (FCNC) and CP-violating processes are expected to arise [2], clashing with the large amount of accurate experimental data now available on these transitions. This is due to the presence of additional sources of flavour and CP violation beyond the CKM matrix (see for example Ref. [3] for the supersymmetry case).

In general, the flavour puzzle admits two classes of possible solutions. The first one contains models in which a flavour symmetry is invoked to explain the hierarchy of quark masses and mixing angles. These models are based on different theoretical approaches (supersymmetry, grand unification, extra dimensions, ...) leading to different levels of agreement with the data and to different low-energy signals. However, low-energy processes generally receive sizable additional contributions which jeopardize the validity of the SM UT analysis (see Ref. [4] for a supersymmetric example). A generalized UT fit allowing for the presence of arbitrary New Physics (NP) contributions is therefore very useful for model building, since it provides at the same time the allowed ranges for the SM CKM parameters and for the NP contributions to $|\Delta F| = 2$ processes. This will be the subject of the first part of the present work (Secs. 2-4).

The second class of solutions to the flavour puzzle contains models with Minimal Flavour Violation (MFV). The basic idea of MFV is that the only source of flavour violation is in the SM Yukawa couplings, so that all FCNC and CP-violating phenomena can be expressed in terms of the CKM matrix and the top quark Yukawa coupling [5-7]. This leads to strong correlations between different observables, and allows for a detailed study of low-energy phenomena. While there are several implementations of MFV in different contexts (two-Higgs doublet models, supersymmetry [8], extra dimensions [9], ...), it is possible to perform two very general analyses under the MFV hypothesis. The first is the determination of the so-called Universal Unitarity Triangle (UUT) [5], which is a UT fit performed using only quantities that are independent of NP contributions within MFV models. The second is a simultaneous fit of the UT and of NP contributions in the $|\Delta F| = 2$ sector. These two analyses will be presented in the second part of this work (Sec. 5), and they serve as the starting point for the study of rare decays and CP violation in MFV models [10].

Finally, in Sec. 6 we present the possible future improvements in the above analyses by considering a “year 2010” scenario for experimental data and theoretical inputs in the flavour sector.

While to our knowledge the determination of the UUT is presented in this work for the first time, several attempts have been previously made in the study of the UT in the

presence of NP. Considering only model-independent analyses, in Ref. [11] the case of NP contributions to $|\Delta B| = 2$ or $|\Delta S| = 2$ transitions was analyzed: this corresponds to the discussion in Section 4 of the present work. A first version of the present analysis, with some experimental constraints missing, was presented in Ref. [12]. Constraints on NP in the $|\Delta B| = 2$ sector using B physics only were considered in Refs. [13–15]. The determination of the UT from tree-level processes only was presented in Ref. [1]. A general analysis was recently performed in Ref. [16], but not all available constraints were used. With respect to these previous studies, we improve several theoretical aspects and perform a simultaneous determination of UT and NP parameters using all the available constraints in all sectors.

A compilation of the experimental and theoretical inputs to our analyses is presented in Table 1.

Parameter	Value	Gaussian (σ)	Uniform (half-width)
λ	0.2258	0.0014	-
$ V_{cb} $ (excl.)	41.3×10^{-3}	1.0×10^{-3}	1.8×10^{-3}
$ V_{cb} $ (incl.)	41.6×10^{-3}	0.7×10^{-3}	-
$ V_{ub} $ (excl.)	38.0×10^{-4}	2.7×10^{-4}	4.7×10^{-4}
$ V_{ub} $ (incl.)	43.9×10^{-4}	2.0×10^{-4}	2.7×10^{-4}
Δm_d [ps $^{-1}$]	0.501	0.005	-
Δm_s [ps $^{-1}$]	> 14.5 at 95% C.L.	sensitivity 18.3	
$F_{B_s} \sqrt{\hat{B}_{B_s}}$ [MeV]	276	38	-
$\xi = \frac{F_{B_s} \sqrt{\hat{B}_{B_s}}}{F_{B_d} \sqrt{\hat{B}_{B_d}}}$	1.24	0.04	0.06
\hat{B}_K	0.79	0.04	0.09
ε_K	2.280×10^{-3}	0.013×10^{-3}	-
f_K [MeV]	160	fixed	
Δm_K [ps $^{-1}$]	0.5301×10^{-2}	fixed	
$\sin 2\beta$	0.687	0.032	-
\overline{m}_t [GeV]	163.8	3.2	-
\overline{m}_b [GeV]	4.21	0.08	-
\overline{m}_c [GeV]	1.3	0.1	-
$\alpha_s(M_Z)$	0.119	0.003	-
G_F [GeV $^{-2}$]	1.16639×10^{-5}	fixed	
m_W [GeV]	80.425	fixed	
$m_{B_d^0}$ [GeV]	5.279	fixed	
$m_{B_s^0}$ [GeV]	5.375	fixed	
m_K^0 [GeV]	0.4977	fixed	

Table 1: *Values of the relevant quantities used in the UT fit. The Gaussian and the flat contributions to the uncertainty are given in the third and fourth columns respectively (for details on the statistical treatment see Ref. [17]). Several branching ratios and CP asymmetries have been used. Their values and errors can be found in Ref. [18] and have been updated to Summer 2005.*

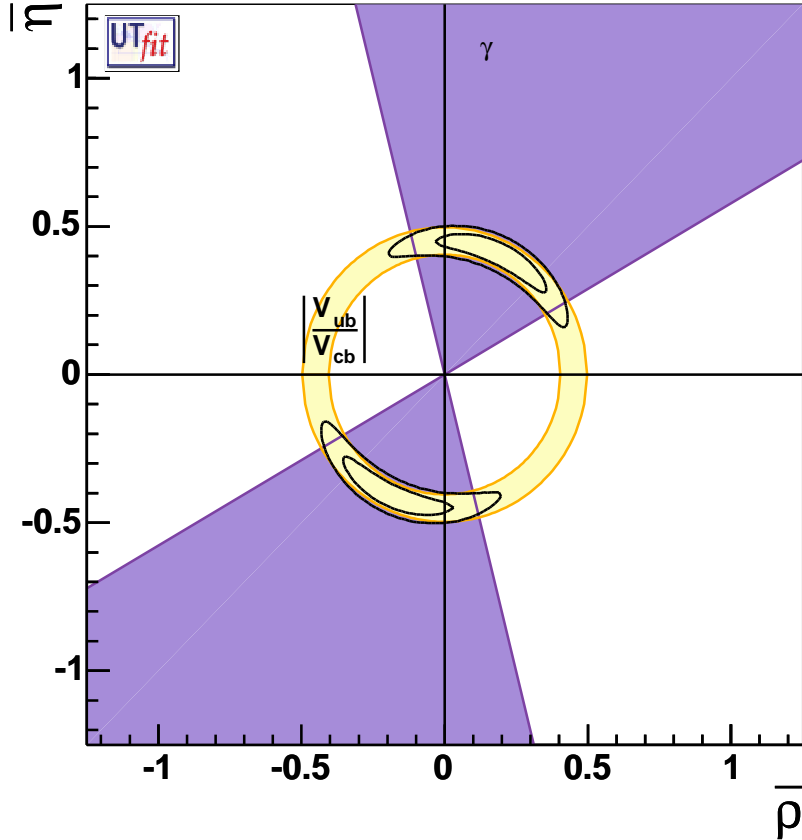


Figure 1: The selected region on $\bar{\rho}-\bar{\eta}$ plane obtained from the determination of $|V_{ub}/V_{cb}|$ and γ (using DK final states). Selected regions corresponding to 68% and 95% probability are shown, together with 95% probability regions for γ and $|V_{ub}/V_{cb}|$.

2 Unitarity clock, unitarity hands: A model-independent determination of the UT

Let us first of all discuss the shape of the UT in the presence of arbitrary NP contributions. All the available experimental data exclude the possibility of sizable contributions to tree-level SM processes, so that extensions of the SM in which NP enters low-energy processes at the tree level are strongly disfavoured. We can therefore safely assume in this work that NP enters observables in the flavour sector only at the loop level. It is then possible to determine two regions in the $\bar{\rho}-\bar{\eta}$ plane independently of NP contributions, using only tree-level B decays. The CKM elements V_{ub} and V_{cb} are determined using semileptonic inclusive and exclusive B decays. The angle γ is obtained by measuring the phase of V_{ub} appearing in the interference between $b \rightarrow c$ and $b \rightarrow u$ transitions to DK final states.¹

¹We neglect possible NP contributions to $D^0-\bar{D}^0$ mixing, since their contribution is expected to be well below the present experimental accuracy [19]. In the future, it might become necessary to take them into account following Ref. [20].

As shown in Fig. 1, it is now lunchtime ($\sim 13:35$) on Andrzej's unitarity clock [21].²

The results of this analysis, reported in Tab. 2, can be used as a reference for model-building and phenomenology in any extension of the SM with loop-mediated contributions to FCNC processes. The present precision is expected to improve considerably in the near future, as discussed in Sec. 6.

UT fit - using only $ V_{ub}/V_{cb} $ and γ		
	SM Solution	2 nd Solution
$\bar{\rho}$	0.18 ± 0.12	-0.18 ± 0.12
$\bar{\eta}$	0.41 ± 0.05	-0.41 ± 0.05
$\sin 2\beta$	0.782 ± 0.065	-0.641 ± 0.087
$\gamma [^\circ]$	65 ± 18	-115 ± 18
$\alpha [^\circ]$	87 ± 15	-46 ± 15
$2\beta + \gamma [^\circ]$	122 ± 13	-152 ± 13

Table 2: *Results for several UT parameters, obtained using the constraints from $|V_{ub}/V_{cb}|$ and γ (using DK final states).*

Beyond the Standard Model, one can include the information from other constraints, taking into account the effect of NP in a general way. In particular, one has to consider two effects:

- The contribution of new operators in the $|\Delta F| = 2$ Hamiltonian, which affects mixing processes and, as a consequence, the determination of $\Delta m_{d,s}$, ε_K and of the angles β and α .
- The effect of NP in the $|\Delta F| = 1$ Hamiltonian, for all those processes occurring through penguin transitions. In our case, this concerns the determination of α from charmless B decays and the CP asymmetry in semileptonic B decays A_{SL} .

3 Model-independent constraints on New Physics in $|\Delta F|=2$ transitions

Our goal in this Section is to use the available experimental information on loop-mediated processes to constrain the NP contributions to $|\Delta F|=2$ transitions. In general, NP models introduce a large number of new parameters: flavour changing couplings, short distance coefficients and matrix elements of new local operators. The specific list and the actual values of these parameters can only be determined within a given model. Nevertheless, each of the mixing processes listed in Tab. 3 is described by a single amplitude and can be parameterized, without loss of generality, in terms of two parameters, which quantify the difference of the complex amplitude with respect to the SM one [22]. Thus, for instance,

²Fig. 1 first appeared in Ref. [1]. Similar results were recently obtained in Ref. [16].

Tree-Level	B_d^0 mixing	K^0 mixing	B_s^0 mixing
$ V_{ub}/V_{cb} $	Δm_d	ϵ_K	Δm_s
$\gamma (DK)$	$A_{CP}(B \rightarrow J/\psi K)$		$A_{CP}(B_s^0 \rightarrow J/\psi \phi)$
	$A_{CP}(B \rightarrow \pi\pi, \rho\pi, \rho\rho)$		
	A_{SL}		

Table 3: *Different processes and corresponding measurements contributing to the determination of $\bar{\rho}$, $\bar{\eta}$, C_{B_d} , ϕ_{B_d} , C_{B_s} , ϕ_{B_s} and C_{ϵ_K} . Δm_K is not considered due to the fact that the long distance effects are not well under control.*

in the case of $B_q^0 - \bar{B}_q^0$ mixing we define

$$C_{B_q} e^{2i\phi_{B_q}} = \frac{\langle B_q^0 | H_{\text{eff}}^{\text{full}} | \bar{B}_q^0 \rangle}{\langle B_q^0 | H_{\text{eff}}^{\text{SM}} | \bar{B}_q^0 \rangle}, \quad (q = d, s) \quad (1)$$

where $H_{\text{eff}}^{\text{SM}}$ includes only the SM box diagrams, while $H_{\text{eff}}^{\text{full}}$ includes also the NP contributions.³ In the absence of NP effects, $C_{B_q} = 1$ and $\phi_{B_q} = 0$ by definition. The experimental quantities determined from the $B_q^0 - \bar{B}_q^0$ mixings and listed in Tab. 3 are related to their SM counterparts and the NP parameters by the following relations:

$$\Delta m_d^{\text{exp}} = C_{B_d} \Delta m_d^{\text{SM}}, \quad \sin 2\beta^{\text{exp}} = \sin(2\beta^{\text{SM}} + 2\phi_{B_d}), \quad \alpha^{\text{exp}} = \alpha^{\text{SM}} - \phi_{B_d}, \quad (2)$$

in a self-explanatory notation. As far as the $K^0 - \bar{K}^0$ mixing is concerned, we find it convenient to introduce a single parameter which relates the imaginary part of the amplitude to the SM one:

$$C_{\epsilon_K} = \frac{\text{Im}[\langle K^0 | H_{\text{eff}}^{\text{full}} | \bar{K}^0 \rangle]}{\text{Im}[\langle K^0 | H_{\text{eff}}^{\text{SM}} | \bar{K}^0 \rangle]}. \quad (3)$$

This definition implies in fact a simple relation for the measured value of ϵ_K ,

$$\epsilon_K^{\text{exp}} = C_{\epsilon_K} \epsilon_K^{\text{SM}} \quad (K^0 - \bar{K}^0 \text{ mixing}). \quad (4)$$

Δm_K is not considered because the long distance effects are not well under control. Therefore, all NP effects which enter the present analysis are parameterized in terms of three real quantities, C_{B_d} , ϕ_{B_d} , and C_{ϵ_K} . NP in the B_s sector is not considered in this case, due to the lack of experimental information, since both Δm_s and $A_{CP}(B_s \rightarrow J/\psi \phi)$ are not measured yet.

3.1 New Physics effects in the extraction of α from $|\Delta F|=1$ processes

In principle, the extraction of α from $B \rightarrow \pi\pi, \rho\pi, \rho\rho$ decays is affected by NP effects in $|\Delta F|=1$ transitions. Actually, in the presence of NP in the strong $b \rightarrow d$ penguins, the decay amplitudes for B mesons decaying into $\pi\pi, \rho\pi$ and $\rho\rho$ are a simple generalization

³We assume here and in the following that NP only affects the dispersive part of the effective Hamiltonian.

of the SM ones (given for example in Eqs. (17) and (18) of Ref. [1]): Assuming that NP modifies significantly only the “penguin” amplitude P without changing its isospin quantum numbers (i.e. barring large isospin-breaking NP effects), the only necessary modification amounts to adding an arbitrary weak phase to P . For example, the amplitudes of $B \rightarrow \pi\pi(\rho\rho)$ can be written as

$$\begin{aligned} A^{+-} &= -Te^{-i\alpha} + Pe^{i\phi_P}e^{i\delta_P} \\ A^{+0} &= -\frac{1}{\sqrt{2}} \left[e^{-i\alpha} (T + T_c e^{i\delta_{Tc}}) \right] \\ A^{00} &= -\frac{1}{\sqrt{2}} \left[T_c e^{-i\alpha} e^{i\delta_{Tc}} + Pe^{i\phi_P}e^{i\delta_P} \right], \end{aligned} \quad (5)$$

where T , T_c and P are real parameters, δ_P and δ_{Tc} are strong phases, α is the angle of the UT, and ϕ_P is an additional weak phase due to the presence of NP. From Eq. (5) it is obvious that the procedure to extract α is exactly the same as in the SM: one constrains the penguin parameter using the BR ’s and then estimates the uncertainty on α coming from the penguin pollution.

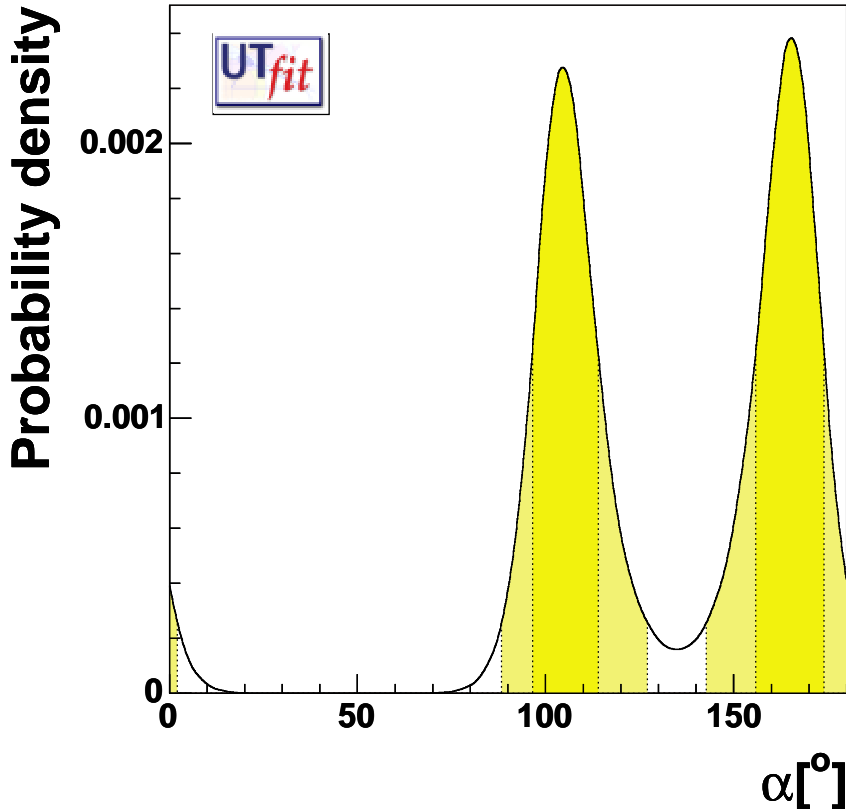


Figure 2: *P.d.f. of α from the combination of isospin analyses of $\pi\pi$, $\rho\pi$ and $\rho\rho$ decay modes, including NP effects in the $|\Delta F| = 1$ Hamiltonian.*

The procedure to extract α is exactly the same as in the SM [1], with an expected weaker bound due to the presence of one (two) extra parameter(s) for $\pi\pi$ and $\rho\rho$ ($\rho\pi$).

The experimental information available nowadays is sufficient to constrain α from the combination of the three decays,⁴ even in the presence of NP, as shown in Fig. 2. Here and in the following figures, dark (light) areas correspond to the 68% (95%) probability region. One should notice that these analyses bound α through the quantity $\pi - \beta - \gamma$, where γ comes from the decay amplitudes and β from $B_d - \bar{B}_d$ mixing. Therefore, in the presence of NP effects in the $|\Delta F| = 2$ Hamiltonian, this bound should be regarded as a constraint on $\alpha^{\text{SM}} - \phi_{B_d}$ (see Eq. 2).

3.2 A_{SL} : general considerations and the inclusion of $|\Delta F|=1$ New Physics effects

One can also add the constraint coming from the CP asymmetry in semileptonic B decays A_{SL} , defined as

$$A_{\text{SL}} \equiv \frac{\Gamma(\bar{B}^0 \rightarrow \ell^+ X) - \Gamma(B^0 \rightarrow \ell^- X)}{\Gamma(\bar{B}^0 \rightarrow \ell^+ X) + \Gamma(B^0 \rightarrow \ell^- X)}. \quad (6)$$

It has been noted in Ref. [13] that, even though the present experimental bound is not precise enough to bound $\bar{\rho}$ and $\bar{\eta}$ in the Standard Model, A_{SL} is a crucial ingredient of the UT analysis once the formulae are generalized according to Eq. (2), since this is the only constraint that depends on both C_{B_d} and ϕ_{B_d} :

$$A_{\text{SL}} = -\text{Re} \left(\frac{\Gamma_{12}}{M_{12}} \right)^{\text{SM}} \frac{\sin 2\phi_{B_d}}{C_{B_d}} + \text{Im} \left(\frac{\Gamma_{12}}{M_{12}} \right)^{\text{SM}} \frac{\cos 2\phi_{B_d}}{C_{B_d}}, \quad (7)$$

where Γ_{12} and M_{12} are the absorptive and dispersive parts of the $B_d^0 - \bar{B}_d^0$ mixing amplitude. At the leading order, A_{SL} is independent of penguin operators, and therefore it is also independent of NP in $|\Delta F| = 1$ processes. However, at the NLO, the penguin contribution should be taken into account. In the SM, the effect of penguin operators is GIM suppressed since their CKM factor is aligned with M_{12} : both are proportional to $(V_{tb}^* V_{td})^2$. This is not true anymore in the presence of NP, so that the effects of penguins are amplified beyond the SM and the approximation made in Ref. [13] of neglecting this contribution is questionable. For our analysis of A_{SL} , we therefore start from the full NLO calculation of Ref. [23], allowing for an additional NP contribution to the penguin term in the $|\Delta F| = 1$ amplitude. This introduces two additional parameters (C_{Pen} and ϕ_{Pen}), encoding NP contributions to the penguin part in analogy to what C_{B_d} and ϕ_{B_d} do for the box contribution. Since the penguin amplitude is $\mathcal{O}(\alpha_s)$ with respect to the leading contribution, these parameters introduce a smearing in the theoretical determination of A_{SL} . The generalized expression of A_{SL} is given by

$$\begin{aligned} A_{\text{SL}} = & \frac{2\kappa}{C_{B_d}} \left\{ \sin(2\phi_{B_d}) \left(n_1 + \frac{n_6 B_2 + n_{11}}{B_1} \right) - \frac{\sin(\beta + 2\phi_{B_d})}{R_t} \left(n_2 + \frac{n_7 B_2 + n_{12}}{B_1} \right) \right. \\ & + \frac{\sin(2(\beta + \phi_{B_d}))}{R_t^2} \left(n_3 + \frac{n_8 B_2 + n_{13}}{B_1} \right) + \sin(\phi_{\text{Pen}} + 2\phi_{B_d}) C_{\text{Pen}} \left(n_4 + n_9 \frac{B_2}{B_1} \right) \\ & \left. - \sin(\beta + \phi_{\text{Pen}} + 2\phi_{B_d}) \frac{C_{\text{Pen}}}{R_t} \left(n_5 + n_{10} \frac{B_2}{B_1} \right) \right\} \end{aligned} \quad (8)$$

⁴Using the determination of BR's and CP asymmetry parameters, one has 6 (5) experimental bounds for $\pi\pi$ ($\rho\rho$), to determine five SM unknowns and ϕ_P . In the case of $\rho\pi$, one can use 13 experimental observables to constrain the 9 SM parameters and the additional weak phases of the two penguin amplitudes.

n_1	0.1797 ± 0.0017	n_2	0.1391 ± 0.0193	n_3	-0.0012 ± 0.0014
n_4	-0.0074 ± 0.0020	n_5	0.0020 ± 0.0007	n_6	1.0116 ± 0.0826
n_7	0.0455 ± 0.0144	n_8	-0.0004 ± 0.0046	n_9	-0.0714 ± 0.0170
n_{10}	-0.0041 ± 0.0016	n_{11}	-0.3331 ± 0.2178	n_{12}	0.0028 ± 0.0101
n_{13}	-0.0036 ± 0.0033				

Table 4: *Magic numbers for the calculation of A_{SL} . The quoted errors correspond to Gaussian distributions.*

where B_1 corresponds to the usual B_d parameter for $B^0 - \bar{B}^0$ mixing, $B_2 = 0.84 \pm 0.07$ (flat) [24], $R_t = \sqrt{(1 - \bar{\rho})^2 + \bar{\eta}^2}$ is the length of one of the UT sides, κ is defined in Ref. [23] and the magic numbers n_i are given in Tab. 4. The Standard Model expression can be recovered in the limit $C_X \rightarrow 1$ and $\phi_X \rightarrow 0$ (where $X = B_d$, Pen). Eq. (8) contains NLO QCD and $1/m_b$ corrections; the latter have been estimated using matrix elements computed in the vacuum insertion approximation, since lattice results are not available.

To display the main phenomenological consequences of A_{SL} , let us consider a simplified formula obtained by setting all magic numbers to their central values, and dropping all those smaller than 10^{-2} . In this way we get

$$A_{\text{SL}} \sim \frac{2\kappa}{C_{B_d}} \left\{ \sin(2\phi_{B_d}) \left(0.18 + \frac{1.01B_2 - 0.33}{B_1} \right) - \frac{\sin(\beta + 2\phi_{B_d})}{R_t} \left(0.14 + 0.05 \frac{B_2}{B_1} \right) \right. \\ \left. + \sin(\phi_{\text{Pen}} + 2\phi_{B_d}) C_{\text{Pen}}(-0.07) \frac{B_2}{B_1} \right\}. \quad (9)$$

The SM penguin contribution vanishes at this level of accuracy. It is evident from the simplified expression in Eq. (9) that the phase ϕ_{B_d} can induce an order-of-magnitude enhancement of A_{SL} relative to the SM, while the penguin phase ϕ_{Pen} can induce corrections comparable to the SM contribution. To be conservative, for our analysis we varied C_{Pen} in the range $[0, 2]$ with $\phi_{\text{Pen}} \in [0, 2\pi]$. This produces only a minor smearing of the dominant effects due to NP in $|\Delta B| = 2$ transitions.

3.3 Results of the analysis and constraints on $|\Delta\mathbf{F}| = 2$ NP contributions

C_{B_d} , ϕ_{B_d} and C_{ϵ_K} are fitted together with $\bar{\rho}$ and $\bar{\eta}$, using the experimental information on $|V_{ub}/V_{cb}|$, $B \rightarrow DK$ decays (γ), ϵ_K , $B \rightarrow \rho\rho$, $\rho\pi$, and $\pi\pi$ decays (α), $B \rightarrow J/\Psi K^{(*)}$ and $B \rightarrow D^0 h^0$ decays [25, 26] (β), and A_{SL} [18]. The output p.d.f.'s for C_{B_d} , C_{ϵ_K} , C_{B_d} vs. ϕ_{B_d} , and γ vs. ϕ_{B_d} are shown in Fig. 3, and the corresponding regions in the $\bar{\rho}$ – $\bar{\eta}$ plane are presented in Fig. 4.

It is important to remark that the constraints coming from the experimental observables allow for an increase in the precision on $\bar{\rho}$ and $\bar{\eta}$ with respect to the pure tree-level determination. This is clear comparing Fig. 1 to Fig. 4.

To illustrate the impact of each experimental constraint on the analysis, in Fig. 5 we show the selected regions in the ϕ_{B_d} vs. C_{B_d} and ϕ_{B_d} vs. γ planes using different combinations of constraints. The first row represents the pre-2004 situation, when only $|V_{ub}/V_{cb}|$, Δm_d , ϵ_K and $\sin 2\beta$ were available, selecting a continuous band for ϕ_{B_d} as a

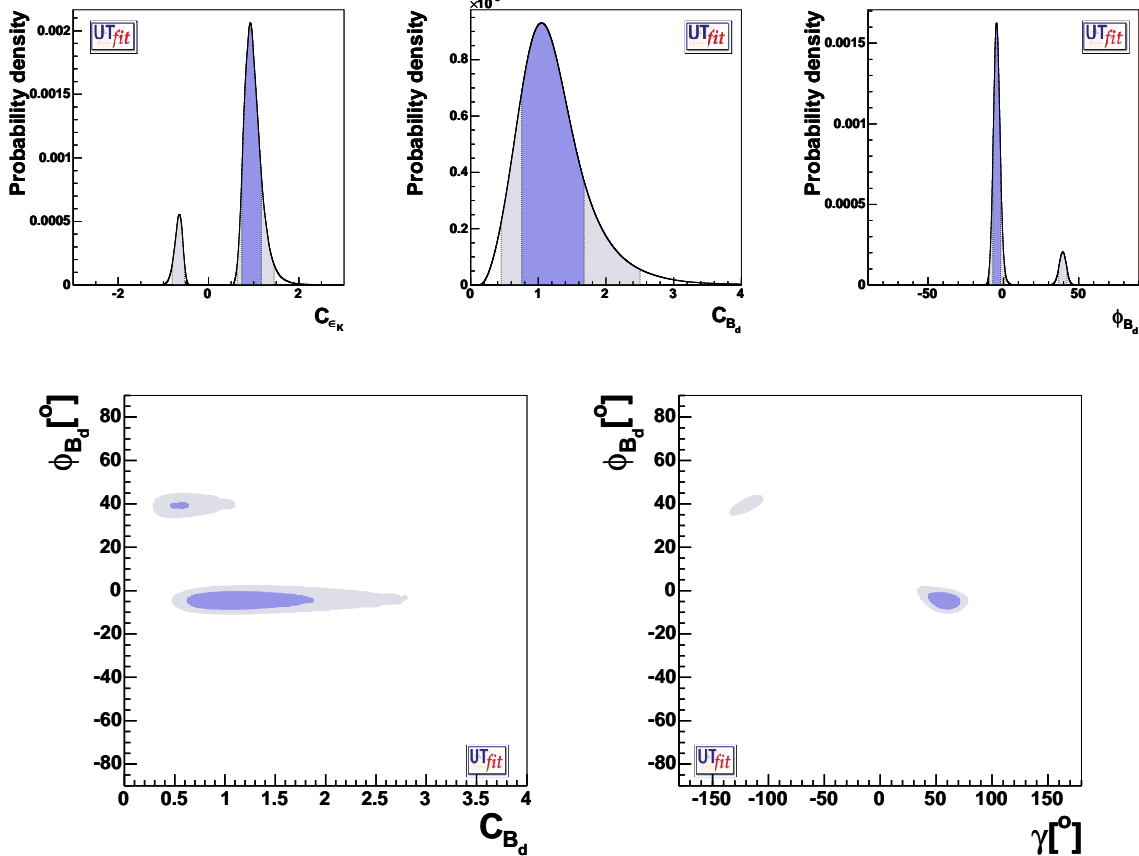


Figure 3: Output P.d.f.'s for C_{ϵ_K} (top-left), C_{B_d} (top-center), ϕ_{B_d} (top-right), and 2D distributions of ϕ_{B_d} vs. C_{B_d} (bottom-left) and ϕ_{B_d} vs. γ . Dark (light) areas correspond to the 68% (95%) probability region.

function of γ and a broad region for C_{B_d} . Adding the determination of γ (second row), only four regions in the ϕ_{B_d} vs. γ plane survive, two of which overlap in the ϕ_{B_d} vs. C_{B_d} plane. Two of these solutions have values of $\cos 2(\beta + \phi_{B_d})$ and $\alpha - \phi_{B_d}$ different from the SM predictions, and are therefore disfavoured by $(\cos 2\beta)^{\text{exp}}$ and by the measurement of $(2\beta)^{\text{exp}}$ from $B \rightarrow D h^0$ decays, and by α^{exp} (third and fourth row respectively). On the other hand, the third solution has a very large value for A_{SL} and is therefore disfavoured by $A_{\text{SL}}^{\text{exp}}$, leading to the final results already presented in Fig. 3.

In Tab. 5 we give the numerical results for the NP parameters and some of the relevant UT quantities, for which we show the output distributions in Fig. 6. A comment is needed for the case of Δm_s : the output distribution reported in Fig. 7 represents the SM contribution only (*i.e.* it corresponds to $C_{B_s} = 1$). Therefore this numerical result should not be taken as a prediction for Δm_s in a general NP scenario in which $C_{B_s} \neq 1$. The conclusion that we can draw from the output distribution of Δm_s is most easily read from the compatibility plot⁵ shown in Fig. 7: a value of $\Delta m_s > 30$ (44) ps^{-1} would imply the presence of NP in $B_s - \bar{B}_s$ mixing at the 2 (3) σ level. On the other hand, from the similar result in the contest of the Standard Model [1] one can still conclude that $\Delta m_s > 29$ (34)

⁵The method used to calculate the level of agreement in the compatibility plot is explained in [1].

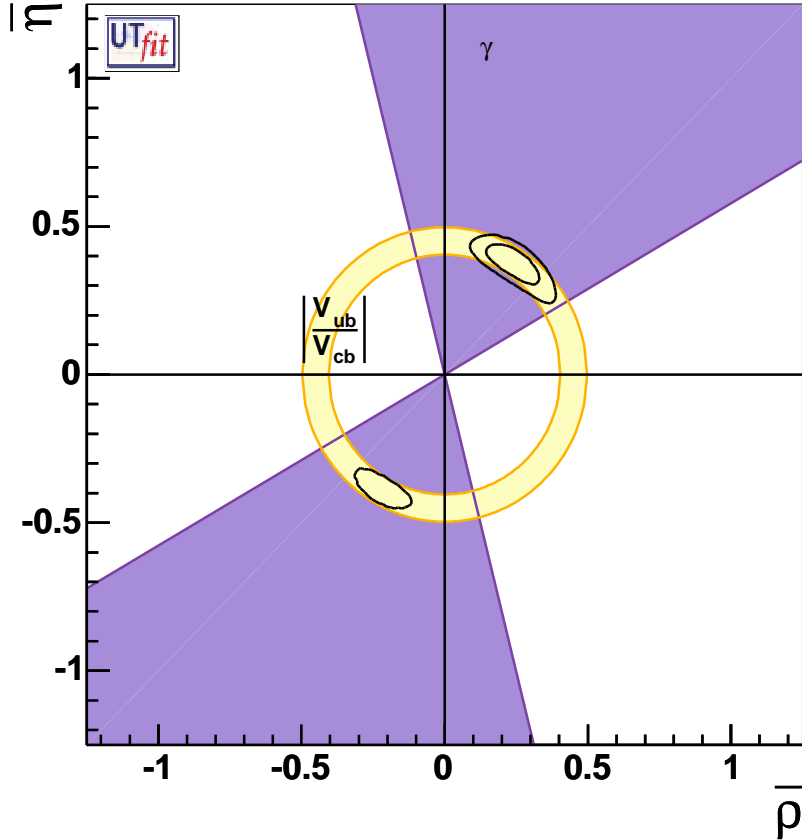


Figure 4: The selected region on $\bar{\rho}$ - $\bar{\eta}$ plane obtained from the NP generalized analysis. Selected regions corresponding to 68% and 95% probability are shown, together with 95% probability regions for γ (from DK final states) and $|V_{ub}/V_{cb}|$.

ps^{-1} would imply the presence of NP at the $2(3)\sigma$ level (but not necessarily in the B_s sector).

Before concluding this section, let us analyze more in detail the results in Fig. 3. Writing

$$C_{B_d} e^{2i\phi_{B_d}} = \frac{A_{\text{SM}} e^{2i\beta} + A_{\text{NP}} e^{2i(\beta + \phi_{\text{NP}})}}{A_{\text{SM}} e^{2i\beta}}, \quad (10)$$

and given the p.d.f. for C_{B_d} and ϕ_{B_d} , we can derive the p.d.f. in the $(A_{\text{NP}}/A_{\text{SM}})$ vs. ϕ_{NP} plane. The result is reported in Fig. 8. We see that the NP contribution can be substantial if its phase is close to the SM phase, while for arbitrary phases its magnitude has to be much smaller than the SM one. Notice that, with the latest data, the SM ($\phi_{B_d} = 0$) is disfavoured at 68% probability due to a slight disagreement between $\sin 2\beta$ and $|V_{ub}/V_{cb}|$. This requires $A_{\text{NP}} \neq 0$ and $\phi_{\text{NP}} \neq 0$. For the same reason, $\phi_{\text{NP}} > 90^\circ$ at 68% probability and the plot is not symmetric around $\phi_{\text{NP}} = 90^\circ$.

Assuming that the small but non-vanishing value for ϕ_{B_d} we obtained is just due to a statistical fluctuation, the result of our analysis points either towards models in which new sources of flavour and CP violation are only present in $b \rightarrow s$ transitions, a well-motivated

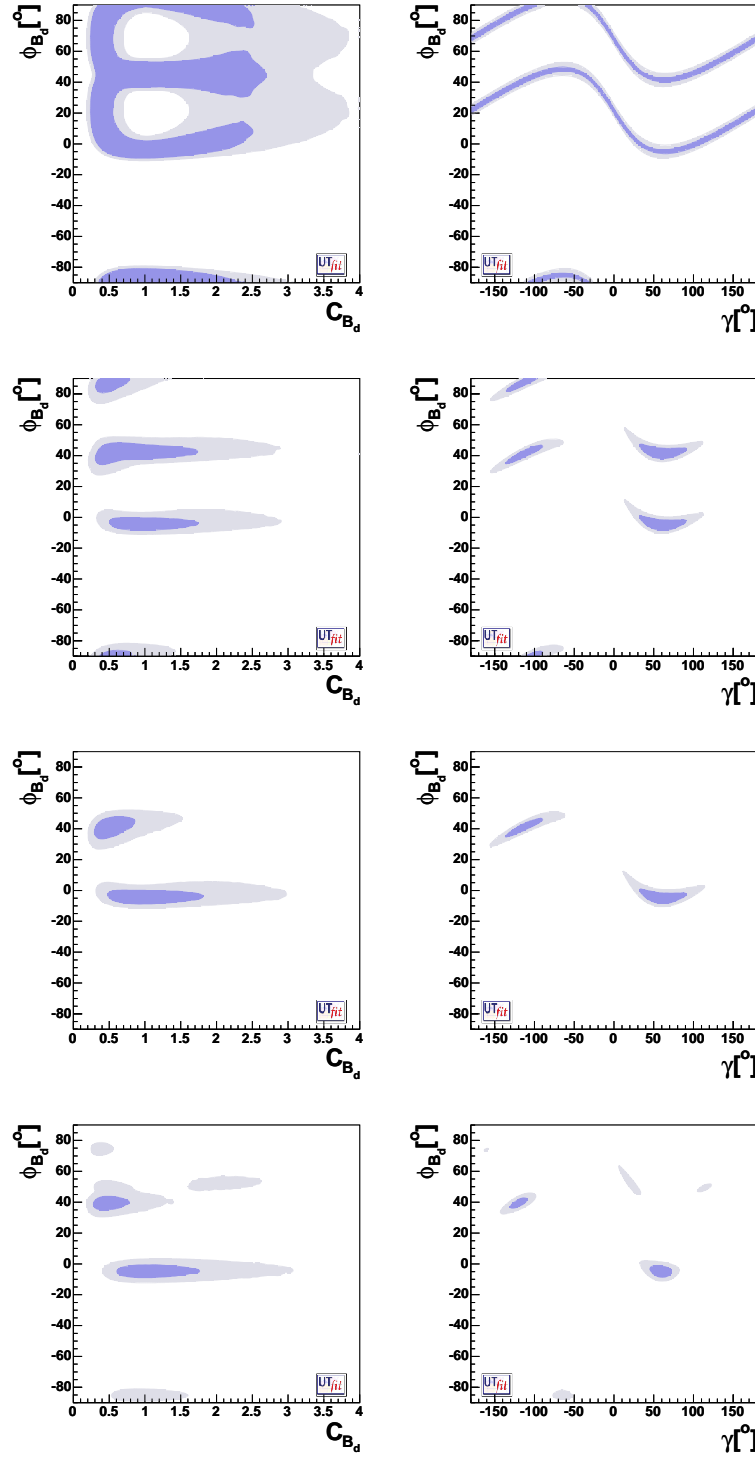


Figure 5: 2D distributions of ϕ_{B_d} vs. C_{B_d} (left) and ϕ_{B_d} vs. γ (right) using the following constraints: i) $|V_{ub}/V_{cb}|$, Δm_d , ε_K and $\sin 2\beta$ (first row); ii) the constraints in i) plus γ (second row); iii) the constraints in ii) plus $\cos 2\beta$ from $B_d \rightarrow J/\psi K^*$ and β from $B \rightarrow D h^0$ (third row); iv) the constraints in ii) plus α (fourth row).

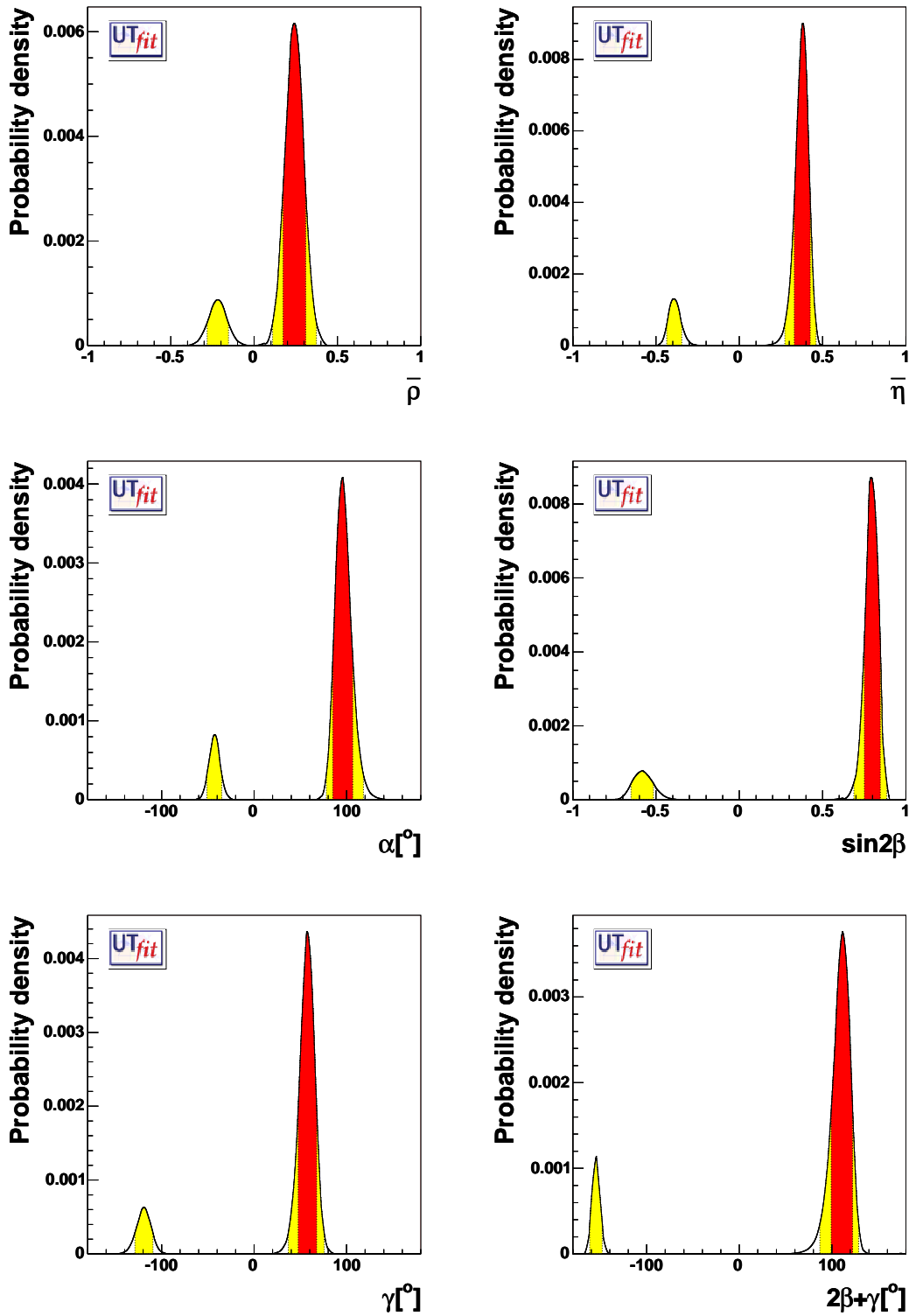


Figure 6: *From top to bottom and from left to right, the p.d.f.'s for $\bar{\rho}$, $\bar{\eta}$, α , $\sin 2\beta$, γ and $2\beta + \gamma$. The red (darker) and the yellow (lighter) zones correspond respectively to 68% and 95% of the area. These results are obtained in the presence of NP in all the processes entering the UT analysis.*

Generalized UTfit analysis in the presence of NP		
	Standard Solution ($\gamma > 0$)	Non-Standard Solution ($\gamma < 0$)
UT parameters		
$\bar{\rho}$	0.242 ± 0.069 ([0.111, 0.374] @95%)	[-0.283, -0.154] @95%
$\bar{\eta}$	0.378 ± 0.048 ([0.273, 0.461] @95%)	[-0.436, -0.346] @95%
$\sin 2\beta$	0.799 ± 0.048 ([0.687, 0.886] @95%)	[-0.650, -0.516] @95%
γ [°]	58 ± 10 ([37, 76] @95%)	[-129, -109] @95%
α [°]	96 ± 11 ([78, 118] @95%)	[-51, -35] @95%
$2\beta + \gamma$ [°]	111 ± 12 ([88, 129] @95%)	[-162, -148] @95%
$\text{Im } \lambda_t$ [$\times 10^{-5}$]	14.8 ± 1.6 ([11.1, 17.7] @95%)	
Δm_s [ps $^{-1}$]	17.6 ± 5.3 ([8.3, 28.7] @95%)	
NP related parameters		
C_{B_d}	1.21 ± 0.46 ([0.45, 2.50] @95%)	
ϕ_{B_d} [°]	-4.5 ± 2.6 ([−9.4, 0.9] @95%)	[36.7, 42.3] @95%
C_{ϵ_K}	0.95 ± 0.22 ([0.64, 1.45] @95%)	[-0.81, -0.53] @95%

Table 5: *Results of the NP generalized analysis on UT parameters. The values for C_{B_d} , ϕ_{B_d} and C_{ϵ_K} are reported. The second solution is excluded at 68% probability level so we quote the 95% ranges only.*

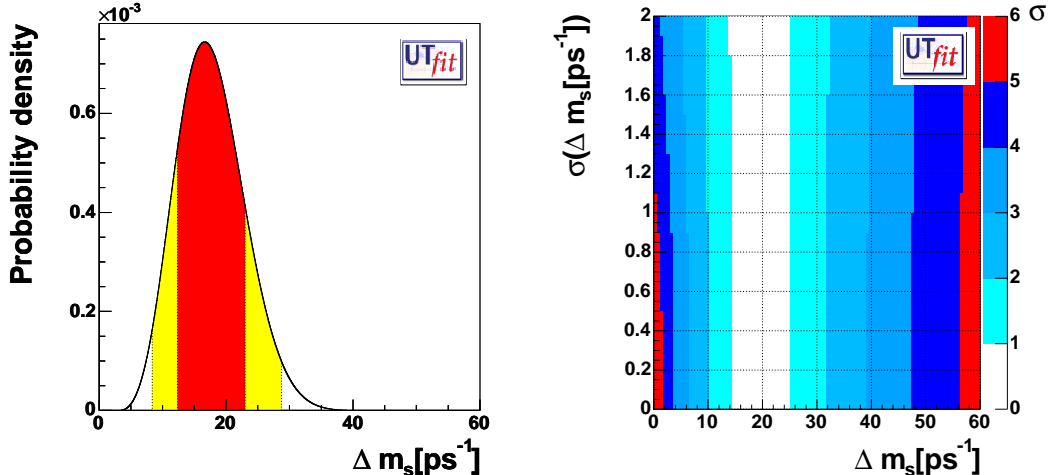


Figure 7: *P.d.f. (left) and compatibility plot (right) for the SM contribution to Δm_s in the presence of NP in all the quantities entering the UT analysis, setting $C_{B_s} = 1$.*

possibility in flavour models and in grand-unified models, or towards models with no new source of flavour and CP violation beyond the ones present in the SM (Minimal Flavour Violation). This second possibility will be studied in detail in Section 5.

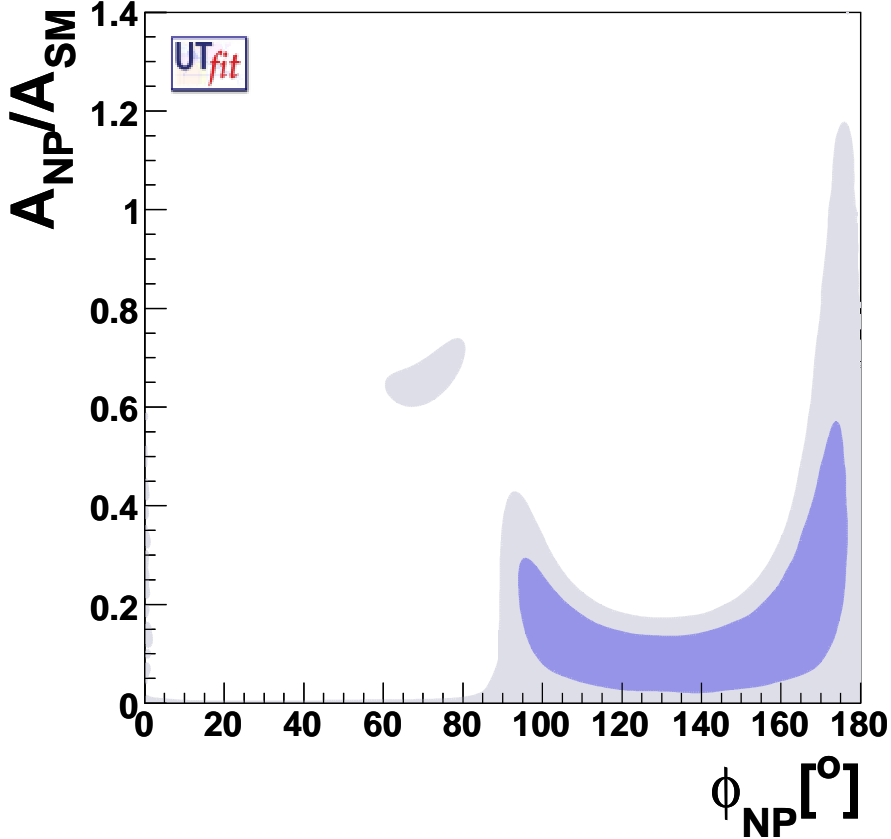


Figure 8: *P.d.f. in the $(A_{\text{NP}}/A_{\text{SM}})$ vs. ϕ_{NP} plane for NP in the $|\Delta B| = 2$ sector (see Eq. (10)).*

4 Constraints on NP from $|\Delta S| = 2$ or $|\Delta B| = 2$ transitions only

A complementary information to the one presented in the previous section is obtained by allowing NP contributions to be present only in $|\Delta S| = 2$ or $|\Delta B| = 2$ transitions. This can be useful to test models beyond the SM in which NP contributions are expected to affect dominantly only one of these two sectors, and is also the starting point to update previous analyses of NP in $|\Delta S| = 2$ or $|\Delta B| = 2$ processes in supersymmetry [27, 28] or in any other given model.

Allowing NP to affect only C_{ε_K} , we obtain the results for the UT parameters, for C_{ε_K} and for $\bar{\rho}$ and $\bar{\eta}$ reported in Fig. 9 and in Tab. 6. The determination of the UT is essentially equivalent to the SM one, since only ε_K is missing in this case.

For the case in which NP only enters $B_d - \bar{B}_d$ mixing, the results are given in Fig. 10 and in Tab. 6. The main difference with the results in the previous section is that one can use ε_K to eliminate the solutions with negative γ .

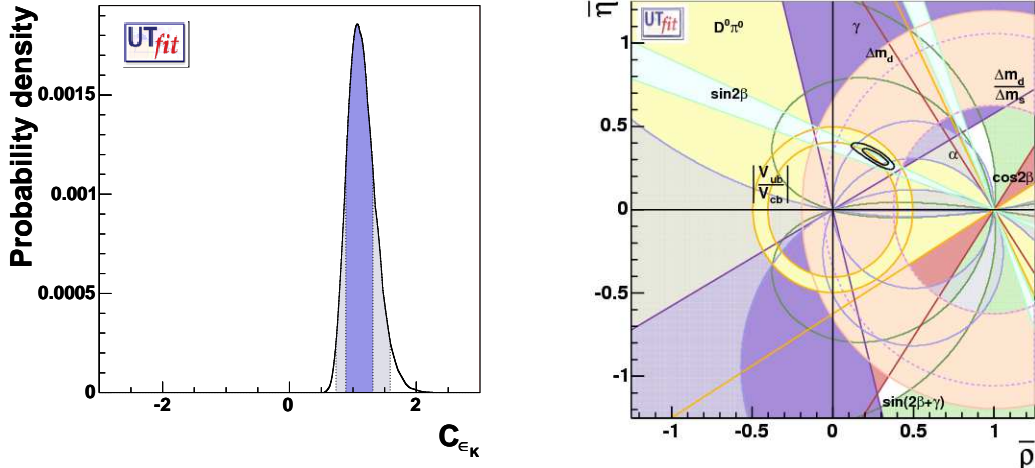


Figure 9: The *p.d.f.* for C_{ϵ_K} (left) and the $\bar{\rho} - \bar{\eta}$ plane (right). In the left plot, the darker and the lighter zones correspond respectively to 68% and 95% of the area. These results are obtained in the presence of NP in $K^0 - \bar{K}^0$ mixing only.

5 Minimal Flavour Violation models

We now specialize to the case of MFV. Making the basic assumption that the only source of flavour and CP violation is in the Yukawa couplings [6], it can be shown that:

1. The phase of $|\Delta B| = 2$ amplitudes is unaffected by NP, and so is the ratio $\Delta m_s/\Delta m_d$. This allows the determination of the Universal Unitarity Triangle independent on NP effects, based on $|V_{ub}/V_{cb}|$, γ , $A_{CP}(B \rightarrow J/\Psi K^{(*)})$, β from $B \rightarrow D^0 h^0$, α , and $\Delta m_s/\Delta m_d$ [5].
2. For one-Higgs-doublet models, and for two-Higgs-doublet models at low $\tan \beta$, all NP effects in the UT analysis amount to a redefinition of the top box contribution to $|\Delta F| = 2$ processes $S_0(x_t) \rightarrow S_0(x_t) + \delta S_0$.
3. For two-Higgs-doublet models with large $\tan \beta$, NP enters in a similar way with respect to the low $\tan \beta$ case, but this time one cannot relate the parameter redefining $S_0(x_t)$ in the B sector to the similar term in the K sector. Therefore, two different redefinitions must be made for the B and K sectors: $S_0(x_t) \rightarrow S_0(x_t) + \delta S_0^{B,K}$.

We perform three different analyses, corresponding to the points 1.-3. above. First, we present the determination of the UUT, which is independent of NP contributions (Sec. 5.1) in the context of MFV models. Then we add to the analysis the NP parameter δS_0 and constrain it, together with $\bar{\rho}$ and $\bar{\eta}$, using also the neutral meson mixing amplitudes. Finally, we consider the case $\delta S_0^B \neq \delta S_0^K$ and determine the constraints on $\bar{\rho}$, $\bar{\eta}$ and these NP parameters.

5.1 Universal Unitarity Triangle

In Fig. 11 we show the allowed region in the $\bar{\rho} - \bar{\eta}$ plane for the UUT, and in Fig. 12 we plot the *p.d.f.*'s for several UT quantities. The corresponding values and ranges are

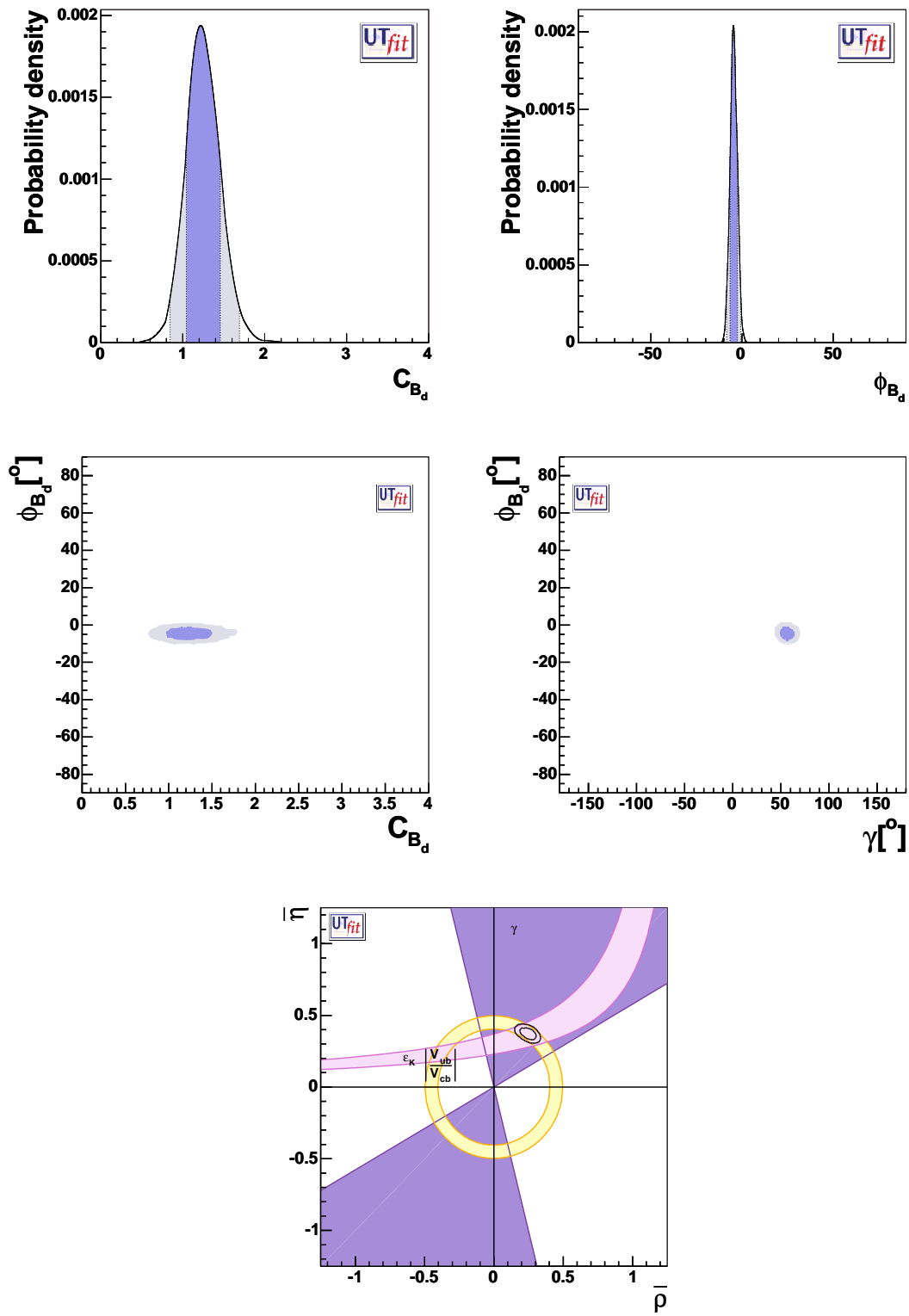


Figure 10: From top to bottom and from left to right, the p.d.f.'s for C_{B_d} , ϕ_{B_d} , ϕ_{B_d} vs. C_{B_d} , ϕ_{B_d} vs. γ and the $\bar{\rho} - \bar{\eta}$ plane. The darker and the lighter zones correspond respectively to 68% and 95% of the area. These results are obtained in the presence of NP in $B_d^0 - \bar{B}_d^0$ mixing only.

Generalized UTfit analysis in the presence of NP		
	$ \Delta S = 2$ only	$ \Delta B_d = 2$ only
UT parameters		
$\bar{\rho}$	$0.267 \pm 0.056 [0.145, 0.368]$	$0.246 \pm 0.038 [0.166, 0.317]$
$\bar{\eta}$	$0.319 \pm 0.034 [0.257, 0.387]$	$0.372 \pm 0.028 [0.318, 0.424]$
$\sin 2\beta$	$0.730 \pm 0.028 [0.674, 0.781]$	$0.794 \pm 0.033 [0.727, 0.854]$
$\gamma [^\circ]$	$50 \pm 9 [35, 69]$	$56 \pm 5 [46, 67]$
$\alpha [^\circ]$	$107 \pm 9 [87, 123]$	$97 \pm 6 [86, 108]$
$2\beta + \gamma [^\circ]$	$100 \pm 10 [80, 118]$	$109 \pm 6 [96, 120]$
$\text{Im } \lambda_t [\times 10^{-5}]$	$12.6 \pm 1.4 [10.1, 15.4]$	$14.9 \pm 1.0 [13.0, 16.8]$
$\Delta m_s [\text{ps}^{-1}]$	$22.6 \pm 4.2 [15.2, 30.8]$	$17.4 \pm 2.0 [14.8, 22.4]$
NP related parameters		
C_{B_d}	1	$1.25 \pm 0.21 [0.84, 1.69]$
$\phi_{B_d} [^\circ]$	0	$-4.6 \pm 2.0 [-8.5, -0.7]$
C_{ϵ_K}	$1.10 \pm 0.21 [0.73, 1.59]$	1

Table 6: *Results of the NP generalized analysis on UT parameters, when only NP contributions to the $|\Delta S| = 2$ (left) and $|\Delta B_d| = 2$ (right) processes are considered. The values for C_{B_d} , ϕ_{B_d} and C_{ϵ_K} are reported. The quoted errors represent 68% [95%] probability ranges.*

reported in Tab. 7. The most important differences with respect to the general case are that i) the lower bound on Δm_s forbids the solution in the third quadrant, and ii) the constraint from $\sin 2\beta$ is now effective, so that we are left with a region very similar to the SM one (for the reader's convenience, we also report results of the SM UT analysis in Tab. 7). The values in Tab. 7 are the starting point for any study of rare decays and CP violation in MFV models. See Ref. [10] for a recent analysis based on the results of this work.

5.2 Constraints on NP contributions in MFV models

We now determine the allowed ranges of NP contributions to $|\Delta F| = 2$ processes, both in the small and large $\tan \beta$ regime. Furthermore, using the conventions of Ref. [6], we quantify the scale of NP that can be probed with the UT analysis.

Let us start by considering MFV models with one Higgs doublet or low/moderate $\tan \beta$. In this case, all NP effects in $|\Delta F| = 2$ transitions are due to the effective Hamiltonian⁶

$$\frac{a}{\Lambda^2} \frac{1}{2} \left(\bar{Q}_L \lambda_{FC} \gamma_\mu Q_L \right)^2, \quad (11)$$

with $(\lambda_{FC})_{ij} = Y_t^2 V_{ti}^* V_{tj}$ for $i \neq j$ and zero otherwise, Y_t the top quark Yukawa coupling, Λ the scale of NP and a an unknown (but real) Wilson coefficient. The value of a can range from order one for strongly interacting extensions of the SM to much smaller

⁶Here and in the rest of this section we follow the notation of Ref. [6].

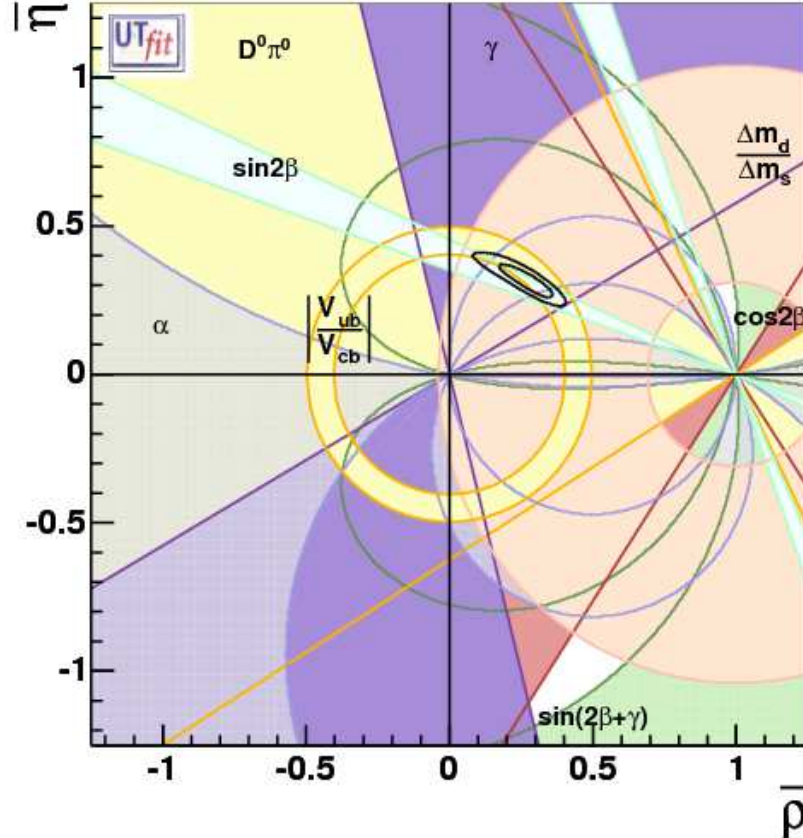


Figure 11: The selected region on $\bar{\rho}$ - $\bar{\eta}$ plane obtained from the determination of the UUT.

values for weakly interacting theories and/or symmetry suppressions analogous to the GIM mechanism in the SM. It is now trivial to project this onto the SM $|\Delta F| = 2$ effective Hamiltonian: it amounts only to a modification of the top quark contribution to box diagrams. Normalizing the NP Wilson coefficient to the SM *effective electroweak scale*⁷ $\Lambda_0 = Y_t \sin^2 \theta_W M_W / \alpha \approx 2.4$ TeV, we obtain

$$S_0(x_t) \rightarrow S_0(x_t) + \delta S_0, \quad \delta S_0 = 4a \left(\frac{\Lambda_0}{\Lambda} \right)^2. \quad (12)$$

We can therefore determine simultaneously the shape of the UT and δS_0 from the standard UT analysis. Then, choosing as reference values $a = \pm 1$, we can translate the constraints on δS_0 into a lower bound on Λ . We obtain (see Fig. 13):

$$\Lambda > \begin{cases} 3.6 \text{ TeV @95\% Prob. for positive } \delta S_0 \\ 5.1 \text{ TeV @95\% Prob. for negative } \delta S_0 \end{cases} \quad (13)$$

Also in this case, we can obtain predictions for UT parameters, together with a constraint on NP contributions (see Tab. 8).

⁷i.e. the scale obtained by writing the SM contribution to $|\Delta F| = 2$ transitions in the form of Eq. (11) with coefficients a of order one.

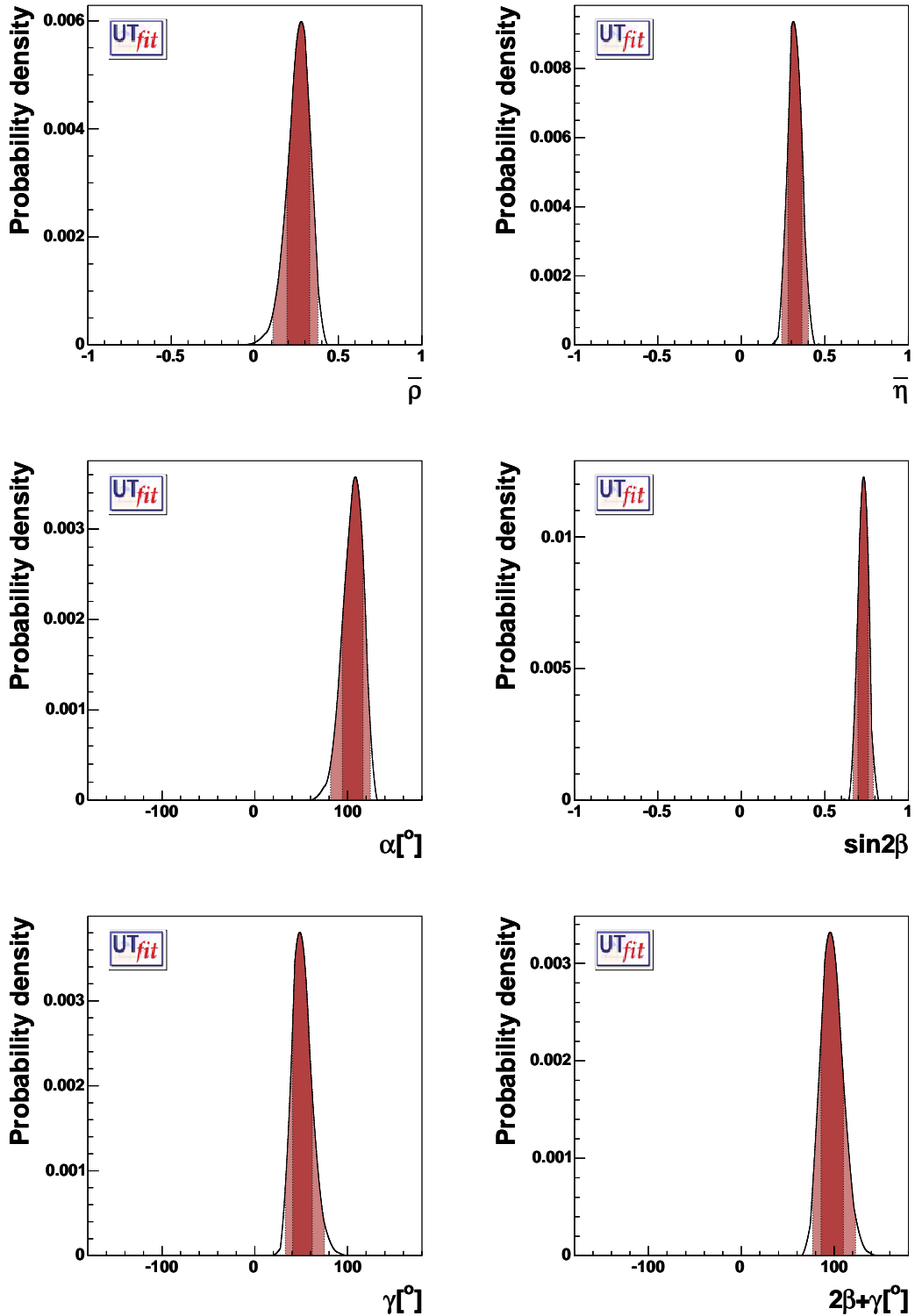


Figure 12: From top to bottom and from left to right, the p.d.f.'s for $\bar{\rho}$, $\bar{\eta}$, α , $\sin 2\beta$, γ and $2\beta + \gamma$. The red (darker) and the yellow (lighter) zones correspond respectively to 68% and 95% of the area. These results are obtained from the UUT analysis.

Universal Unitarity Triangle analysis				
	UUT (68%)	UUT (95%)	SM (68%)	SM (95%)
UT parameters				
$\bar{\rho}$	0.259 ± 0.068	[0.107, 0.376]	0.216 ± 0.036	[0.143, 0.288]
$\bar{\eta}$	0.320 ± 0.042	[0.241, 0.399]	0.342 ± 0.022	[0.300, 0.385]
$\sin 2\beta$	0.728 ± 0.031	[0.668, 0.778]	0.735 ± 0.024	[0.688, 0.781]
$\alpha [^\circ]$	105 ± 11	[81, 124]	98.5 ± 5.7	[87.1, 109.8]
$\gamma [^\circ]$	51 ± 10	[33, 75]	57.6 ± 5.5	[46.8, 68.7]
$(2\beta + \gamma) [^\circ]$	98 ± 12	[77, 123]	105.3 ± 8.1	[89.6, 121.4]
$\text{Im } \lambda_t [\times 10^{-5}]$	12.7 ± 1.7	[9.7, 15.9]	13.5 ± 0.8	[12.0, 15.0]
$\Delta m_s [\text{ps}^{-1}]$	20.6 ± 5.6	[10.6, 32.6]	20.0 ± 1.8	[15.5, 24.2]

Table 7: Results of the UUT analysis. For convenience, the SM results from Ref. [1] are also reported.

Minimal Flavour Violation analysis				
	low/moderate $\tan \beta$		large $\tan \beta$	
	68%	95%	68%	95%
$\bar{\rho}$	0.216 ± 0.058	[0.109, 0.361]	0.231 ± 0.067	[0.112, 0.375]
$\bar{\eta}$	0.351 ± 0.032	[0.265, 0.406]	0.347 ± 0.036	[0.254, 0.404]
$\sin 2\beta$	0.733 ± 0.027	[0.679, 0.781]	0.731 ± 0.027	[0.673, 0.781]
$\alpha [^\circ]$	98.6 ± 9.5	[81.6, 121.7]	101 ± 11	[82, 124]
$\gamma [^\circ]$	57.6 ± 9.1	[35.7, 79.1]	55 ± 11	[34, 74]
$(2\beta + \gamma) [^\circ]$	104 ± 10	[80, 122]	102 ± 12	[77, 121]
$\text{Im } \lambda_t [\times 10^{-5}]$	13.6 ± 1.4	[10.1, 16.0]	13.4 ± 1.9	[9.7, 16.3]
$\Delta m_s [\text{ps}^{-1}]$	19.5 ± 2.6	[15.0, 31.7]	22.6 ± 5.4	[15.5, 35.1]

Table 8: Results for UT parameters from the MFV generalized analysis.

In the case of large $\tan \beta$, the situation changes since the bottom Yukawa coupling is not negligible anymore, and it can distinguish transitions involving b quarks from those involving only light quarks. This spoils the correlation of $|\Delta B| = 2$ with $|\Delta S| = 2$ amplitudes, so that two uncorrelated parameters δS_0^B and δS_0^K are required in this case, to take into account NP contributions to $B_{d,s} - \bar{B}_{d,s}$ and $K - \bar{K}$ mixing. In a global fit, made by using all the available inputs, Δm_d and $\Delta m_d/\Delta m_s$ determine the value of δS_0^B , ε_K fixes δS_0^K , while $\bar{\rho}$ and $\bar{\eta}$ are given by the combination of all the other constraints.

Performing this analysis, we bound the UT parameters as given in Tab. 8, limiting the NP scale to be:

$$\Lambda > \begin{cases} 2.6 \text{ TeV @95\% Prob. for positive } \delta S_0^B \\ 4.9 \text{ TeV @95\% Prob. for negative } \delta S_0^B \end{cases} \text{ from } B_{d,s} - \bar{B}_{d,s} \text{ mixing}$$

$$\Lambda > \begin{cases} 3.2 \text{ TeV @95\% Prob. for positive } \delta S_0^K \\ 4.9 \text{ TeV @95\% Prob. for negative } \delta S_0^K \end{cases} \text{ from } K - \bar{K} \text{ mixing} \quad (14)$$

The output distributions for δS_0^B and δS_0^K are given in Fig. 13.

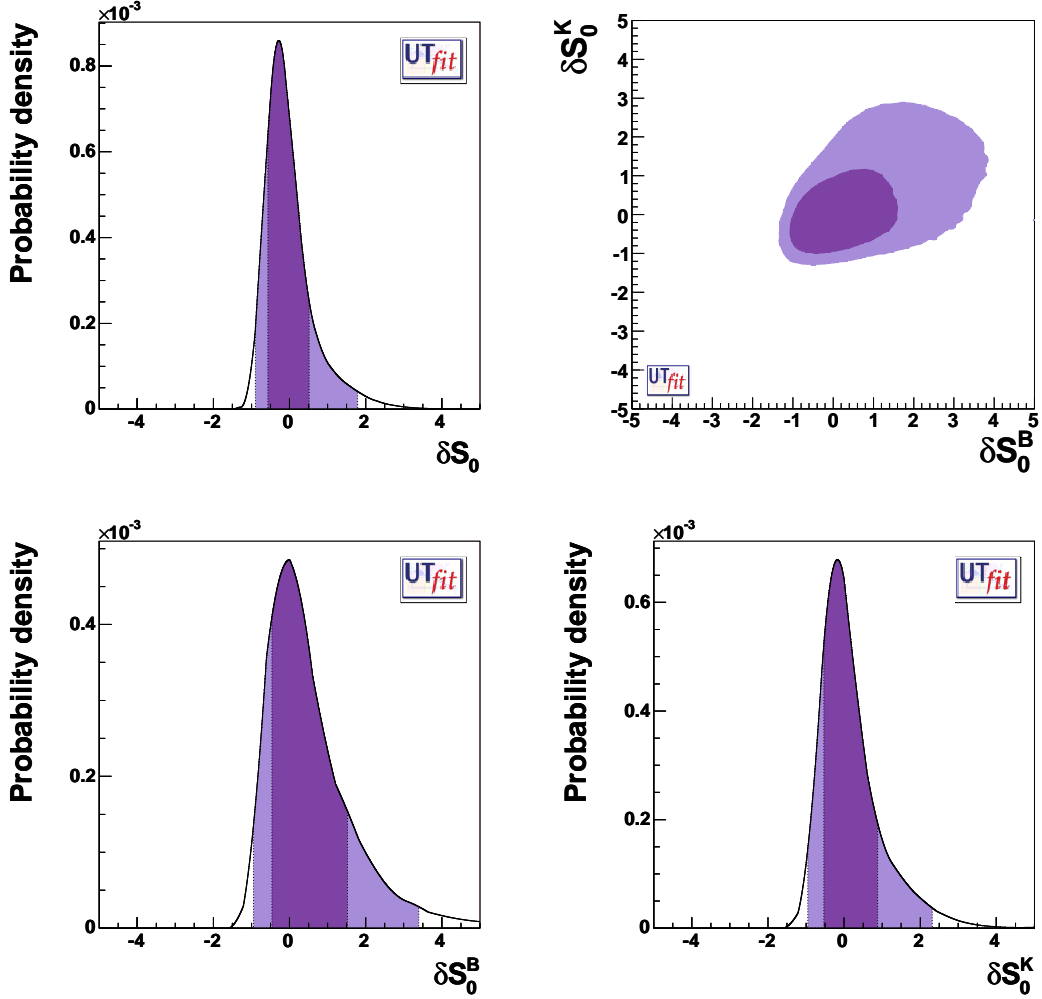


Figure 13: *P.d.f. of δS_0 (top-left), δS_0^K vs δS_0^B (top-right), δS_0^B (bottom-left) and δS_0^K (bottom-right). See the text for details.*

It is instructive to observe the two-dimensional plot of δS_0^B vs. δS_0^K in Fig. 13: within models with only one Higgs doublet or with small $\tan \beta$, the two δ 's are bound to lie on the line $\delta S_0^B = \delta S_0^K$. The correlation coefficient R provides a measure of this relation. We find $R = 0.52$ giving no compelling indication on the value of $\tan \beta$.

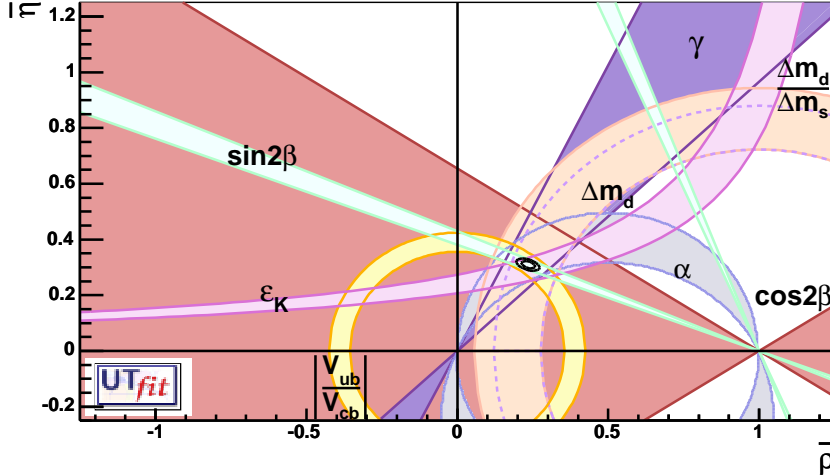


Figure 14: The selected region on $\bar{\rho}$ - $\bar{\eta}$ plane obtained from the Standard Model UT analysis in the “year 2010” scenario.

6 Model Independent constraints on New Physics in the $|\Delta F|=2$ sector in year 2010

We present an exercise on the knowledge of the UT parameters within the generalized NP analysis in a possible scenario in year 2010. At this date, the B factories will have completed their data analysis and the LHCb experiment will have started running.

For this exercise we have assumed a total integrated luminosity for the B factories of 2 ab^{-1} and two years of data taking at LHCb, with an integrated luminosity of 4 fb^{-1} . At that time the lattice community will have produced the final numbers from the Tera-Flops machines. The 2010 projected values and errors for the quantities which are most relevant in UT analysis are given in Tab. 9. Lattice parameters are taken from [29], while the extrapolation of the errors on the experimental measurements is taken from [30–33]. In addition to the improvements of existing measurements, we have added new measurements in the B_s sector from LHCb. In particular the determination of

$$\begin{aligned}
 \Delta m_s^{\text{exp}} &= C_{B_s} \Delta m_s^{\text{SM}} && \text{from } B_s \rightarrow D_s \pi, \\
 \sin 2\chi_s^{\text{exp}} &= \sin(2\chi_s^{\text{SM}} + 2\phi_{B_s}) && \text{from } B_s \rightarrow J/\psi \phi, \\
 (\gamma - 2\chi_s)^{\text{exp}} &= \gamma^{\text{SM}} - 2\chi_s^{\text{SM}} - 2\phi_{B_s} && \text{from } B_s \rightarrow D_s K.
 \end{aligned}$$

The central values for the different observables have been generated in the SM starting from an arbitrarily chosen value of $\bar{\rho}$ and $\bar{\eta}$, so that they are all compatible with each other and the result of the fit is fully “SM like”. The reason for this procedure is to investigate whether, in the “worst case” scenario of perfect confirmation of the SM, one can asymptotically reduce the errors on the NP related quantities introduced in the previous sections, and translate the derived constraint into a lower limit on the energy scale for NP particles. We start from a picture of what the UT analysis should look like in 2010. In Fig. 14 we show the selected region in the $\bar{\rho}$ - $\bar{\eta}$ plane, while in the third column of Tab. 10 we quote the uncertainties on the various quantities from the UT analysis in

Observable	projected value & error
$\sin 2\beta$	0.695 ± 0.010 (1.4%)
$\alpha[^{\circ}]$	104 ± 5
$\gamma[^{\circ}]$ (DK)	54 ± 5
B_K	0.930 ± 0.047 (5%)
$F_{B_s} \sqrt{\hat{B}_{B_s}}$ [MeV]	0.276 ± 0.014 (5%)
ξ	1.200 ± 0.037 (3%)
$ V_{cb} $ -(incl+excl) (10^{-3})	41.7 ± 0.4 (0.9%)
$ V_{ub} $ -(incl+excl) (10^{-4})	36.4 ± 1.6 (4.2%)
Δm_d [ps^{-1}]	0.503 ± 0.003 (0.6%)
m_t [GeV]	171 ± 3.0
λ	0.2240 ± 0.0008
Δm_s [ps^{-1}]	20.5 ± 0.3
$\sin 2\chi_s$ ($J/\psi\phi$)	0.031 ± 0.045
$(\gamma - 2\chi_s)[^{\circ}]$ ($D_s K$)	51 ± 10

Table 9: *Projected values and errors in year 2010 for the most relevant quantities entering in the UT analysis. The central values are chosen such that the constraints are perfectly compatible within the SM.*

the Standard Model. This should be taken as a reference for the approaches beyond the Standard Model that follow.

Moving from the SM analysis to the model independent approach of Sec. 3, we expect in the future a sizable improvement of the knowledge of the NP parameters:

$$\begin{aligned}
 C_{B_d} &= 0.98 \pm 0.14 & \phi_{B_d} &= (-0.1 \pm 1.3)^{\circ} \\
 C_{B_s} &= 0.99 \pm 0.12 & \phi_{B_s} &= (0.0 \pm 1.3)^{\circ} \\
 C_{\epsilon_K} &= 1.00 \pm 0.10
 \end{aligned} \tag{15}$$

as shown in Fig. 15.

In the same future scenario, one can repeat the MFV analysis, both determining UT parameters using the UUT approach and adding the information from (NP sensitive) mixing quantities to bound the NP scale. The expected errors on the relevant UT quantities are summarized in the forth and fifth columns of Tab. 10.

If no evidence of violation of the Standard Model will emerge from B physics in the era of direct NP search at LHC, this generalized approach will replace the present UT analysis as the default procedure. So, it is important to remark the fact that the generalization of the analysis costs an increasing of about 10% of the errors, which is not a huge price to pay if compared to the gain in terms of the larger physics scenario.⁸ In Fig. 16, we give a hint of what the UUT analysis would look like in 2010.

In this framework, one should expect to increase the lower bound on Λ when the NP sensitive quantities are added to the UUT fit. To have a quantitative example of the

⁸Of course, the output error on Δm_s is also affected by the absence of Δm_d in the fit.

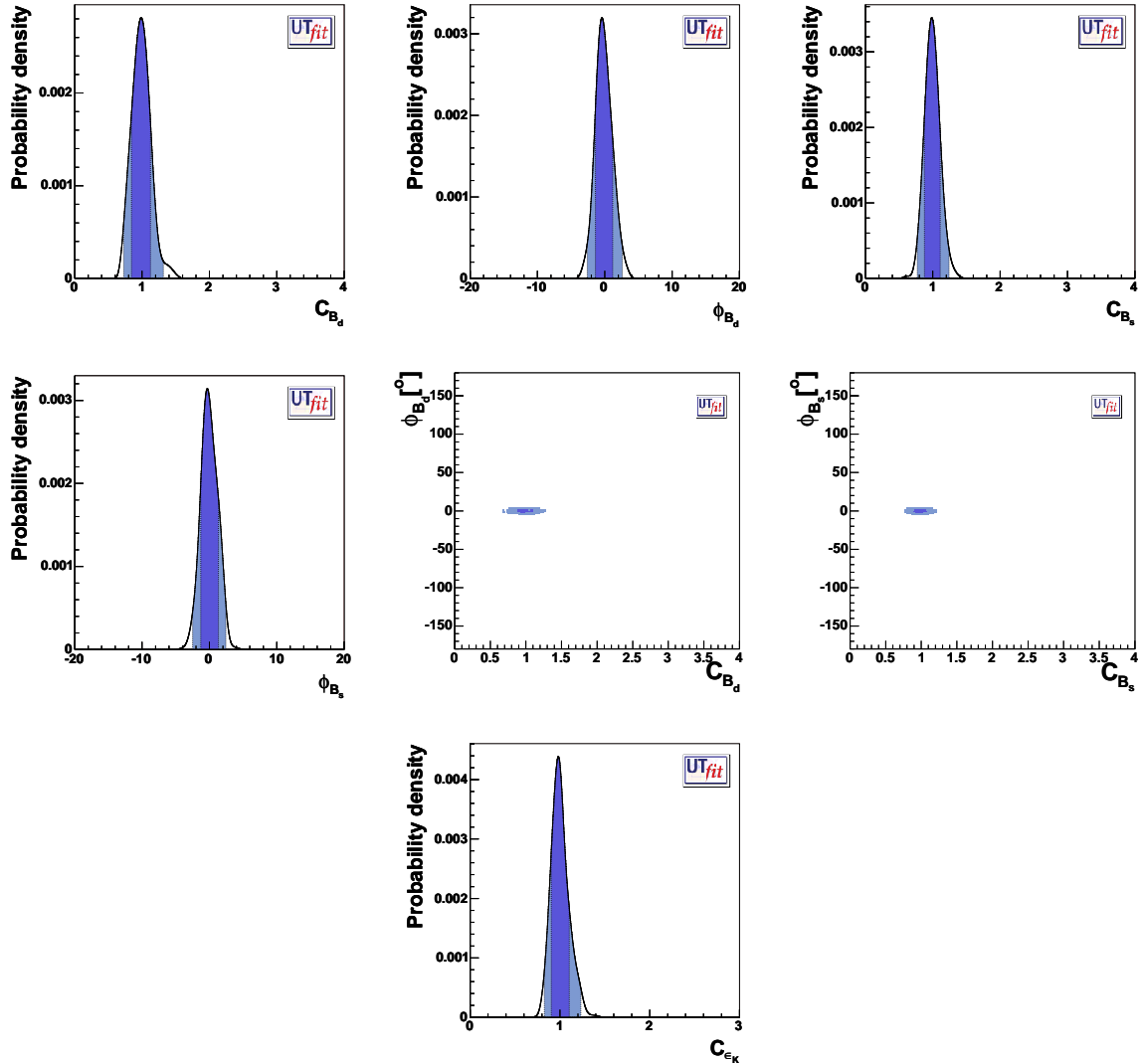


Figure 15: *Projected situation in year 2010. p.d.f. distributions for NP parameters: from top to bottom and from left to right, distributions of C_{B_d} and ϕ_{B_d} , distributions of C_{B_s} and ϕ_{B_s} , 2D distributions of ϕ_{B_d} vs. C_{B_d} and ϕ_{B_s} vs. C_{B_s} , and distribution of C_{ϵ_K} . Dark (light) area corresponds to the 68% (95%) probability region.*

expected improvement, we used the input listed above for the 2010 scenario, obtaining the δS_0 distributions shown in Fig. 17. From these distributions, we get $\Lambda > 7.5(6.6)$ TeV at 95% probability, in the case of positive (negative) value of δS_0 , in the case of MFV models with one Higgs doublet or low/moderate $\tan \beta$. For the case of large $\tan \beta$, we get

$$\begin{aligned} \Lambda &> \begin{cases} 6.0 \text{ TeV @95\% Prob. for positive } \delta S_0^B \\ 6.6 \text{ TeV @95\% Prob. for negative } \delta S_0^B \end{cases} & \text{from } B_{d,s} - \bar{B}_{d,s} \text{ mixing} \\ \Lambda &> \begin{cases} 6.8 \text{ TeV @95\% Prob. for positive } \delta S_0^K \\ 5.1 \text{ TeV @95\% Prob. for negative } \delta S_0^K \end{cases} & \text{from } K - \bar{K} \text{ mixing} \end{aligned} \quad (16)$$

UT analysis in 2010			
Observable	Input error	Output error	
		SM UT	UUT
$\bar{\rho}$	-	0.015	0.021
$\bar{\eta}$	-	0.007	0.010
$\sin 2\beta$	0.010	0.009	0.009
$\alpha [^\circ]$	5	2.1	3.5
$\gamma [^\circ]$	5	2.0	3.2
$2\beta + \gamma [^\circ]$	-	2.3	3.4

Table 10: *Projected uncertainties in year 2010 for the SM UT and the UUT analysis, using all the inputs of Tab. 9.*

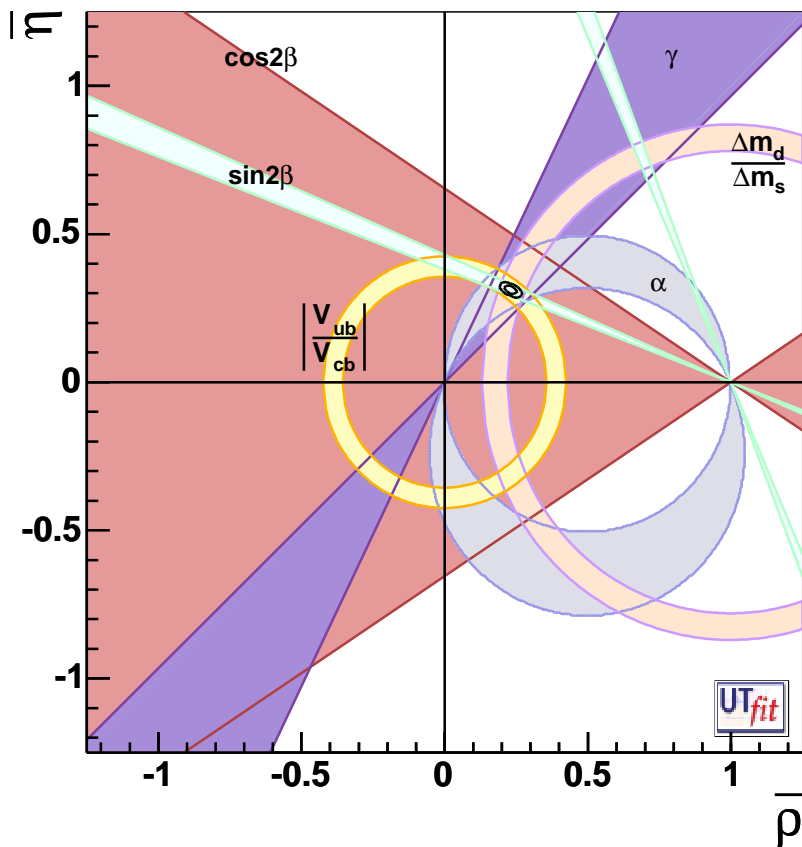


Figure 16: *The selected region on $\bar{\rho}$ - $\bar{\eta}$ plane obtained from the UUT analysis in the “year 2010” scenario.*

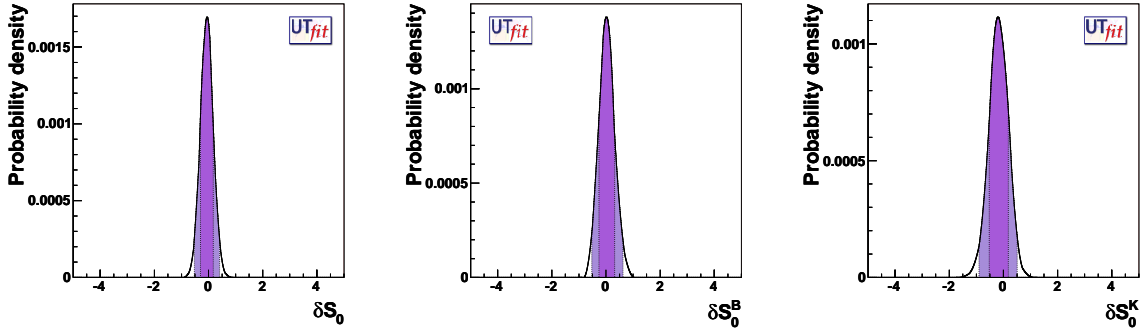


Figure 17: *P.d.f. of δS_0 from MFV fit in the 2010 scenario, in the case of small (left) and large values of $\tan \beta$, from $B_{d,s}$ – $\bar{B}_{d,s}$ (center) and K – \bar{K} (right) mixing.*

7 Conclusions

We have performed a model-independent analysis of the UT in general extensions of the SM with loop-mediated contributions to FCNC processes. Going beyond the pure tree-level determination of the UT already presented in Ref. [1], we have shown how the recent measurements performed at B factories allow for a simultaneous determination of the CKM parameters together with the NP contributions to $|\Delta F| = 2$ processes. We have found strong constraints on NP contributions that can be as large as the SM ones only if the SM and NP amplitudes have the same weak phase.

Motivated by this result, which points towards models with MFV, we have analyzed in detail the UUT. By putting together all the available information, it is possible to determine the UT parameters almost as accurately as in the SM case and to constrain the additional NP parameters. In this way, we probe dimension-six operators up to a scale of 5 TeV, to be compared with the SM reference scale of 2.4 TeV and to the sensitivity of other rare processes, which reaches scales of 9–12 TeV in the case of $b \rightarrow s\gamma$ [6].

Finally, we have presented a possible scenario for the UT analysis in five years from now, taking into account foreseeable progress in theory and experiment, under the pessimistic assumption that the SM perfectly agrees with the data. This exercise allows us to assess the sensitivity to NP that we can expect in the near future. The impressive accuracy we can reach in this kind of analyses shows the great potential of flavour studies in investigating the structure of NP.

References

- [1] M. Bona *et al.* [UTfit Collaboration], JHEP **0507** (2005) 028 [arXiv:hep-ph/0501199].
- [2] F. Gabbiani, E. Gabrielli, A. Masiero and L. Silvestrini, Nucl. Phys. B **477** (1996) 321 [arXiv:hep-ph/9604387].
- [3] L. J. Hall, V. A. Kostelecky and S. Raby, Nucl. Phys. B **267** (1986) 415.
- [4] A. Masiero, M. Piai, A. Romanino and L. Silvestrini, Phys. Rev. D **64** (2001) 075005 [arXiv:hep-ph/0104101].

- [5] A. J. Buras, P. Gambino, M. Gorbahn, S. Jager and L. Silvestrini, Phys. Lett. B **500** (2001) 161 [arXiv:hep-ph/0007085].
- [6] G. D'Ambrosio, G. F. Giudice, G. Isidori and A. Strumia, Nucl. Phys. B **645** (2002) 155 [arXiv:hep-ph/0207036].
- [7] A. J. Buras and R. Buras, Phys. Lett. B **501** (2001) 223 [arXiv:hep-ph/0008273].
 A. J. Buras and R. Fleischer, Phys. Rev. D **64** (2001) 115010 [arXiv:hep-ph/0104238].
 A. J. Buras, Phys. Lett. B **566** (2003) 115 [arXiv:hep-ph/0303060].
 A. J. Buras, Acta Phys. Polon. B **34** (2003) 5615 [arXiv:hep-ph/0310208].
- [8] E. Gabrielli and G. F. Giudice, Nucl. Phys. B **433** (1995) 3 [Erratum-ibid. B **507** (1997) 549] [arXiv:hep-lat/9407029].
 M. Misiak, S. Pokorski and J. Rosiek, Adv. Ser. Direct. High Energy Phys. **15** (1998) 795 [arXiv:hep-ph/9703442].
 M. Ciuchini, G. Degrassi, P. Gambino and G. F. Giudice, Nucl. Phys. B **534** (1998) 3 [arXiv:hep-ph/9806308].
 A. J. Buras, P. H. Chankowski, J. Rosiek and L. Slawianowska, Nucl. Phys. B **659** (2003) 3 [arXiv:hep-ph/0210145].
- [9] T. Appelquist, H. C. Cheng and B. A. Dobrescu, Phys. Rev. D **64** (2001) 035002 [arXiv:hep-ph/0012100].
 A. J. Buras, M. Spranger and A. Weiler, Nucl. Phys. B **660** (2003) 225 [arXiv:hep-ph/0212143].
 A. J. Buras, A. Poschenrieder, M. Spranger and A. Weiler, Nucl. Phys. B **678** (2004) 455 [arXiv:hep-ph/0306158].
- [10] C. Bobeth, M. Bona, A. J. Buras, T. Ewerth, M. Pierini, L. Silvestrini and A. Weiler, arXiv:hep-ph/0505110, accepted by Nucl. Phys. B.
- [11] M. Ciuchini, E. Franco, F. Parodi, V. Lubicz, L. Silvestrini and A. Stocchi, eConf **C0304052** (2003) WG306 [arXiv:hep-ph/0307195].
- [12] M. Pierini in K. Hagiwara, J. Kanzaki and N. Okada, “Supersymmetry and unification of fundamental interactions. Proceedings, 12th International Conference, SUSY 2004, Tsukuba, Japan, June 17-23, 2004.”
- [13] S. Laplace, Z. Ligeti, Y. Nir and G. Perez, Phys. Rev. D **65** (2002) 094040 [arXiv:hep-ph/0202010].
- [14] Z. Ligeti, arXiv:hep-ph/0408267.
- [15] J. Charles *et al.* [CKMfitter Group], Eur. Phys. J. C **41** (2005) 1 [arXiv:hep-ph/0406184].
- [16] F. J. Botella, G. C. Branco, M. Nebot and M. N. Rebelo, Nucl. Phys. B **725** (2005) 155 [arXiv:hep-ph/0502133].

- [17] M. Ciuchini *et al.*, JHEP **0107** (2001) 013 [arXiv:hep-ph/0012308].
- [18] Heavy Flavor Averaging Group,
<http://www.slac.stanford.edu/xorg/hfag/index.html>.
- [19] A. Giri, Y. Grossman, A. Soffer and J. Zupan, Phys. Rev. D **68** (2003) 054018 [arXiv:hep-ph/0303187].
- [20] A. Amorim, M. G. Santos and J. P. Silva, Phys. Rev. D **59** (1999) 056001 [arXiv:hep-ph/9807364].
C. C. Meca and J. P. Silva, Phys. Rev. Lett. **81** (1998) 1377 [arXiv:hep-ph/9807320].
J. P. Silva and A. Soffer, Phys. Rev. D **61** (2000) 112001 [arXiv:hep-ph/9912242].
- [21] A. J. Buras, arXiv:hep-ph/0101336.
- [22] J. M. Soares and L. Wolfenstein, Phys. Rev. D **47** (1993) 1021.
N. G. Deshpande, B. Dutta and S. Oh, Phys. Rev. Lett. **77** (1996) 4499 [arXiv:hep-ph/9608231].
J. P. Silva and L. Wolfenstein, Phys. Rev. D **55** (1997) 5331 [arXiv:hep-ph/9610208].
A. G. Cohen, D. B. Kaplan, F. Lepeintre and A. E. Nelson, Phys. Rev. Lett. **78** (1997) 2300 [arXiv:hep-ph/9610252].
Y. Grossman, Y. Nir and M. P. Worah, Phys. Lett. B **407** (1997) 307 [arXiv:hep-ph/9704287].
- [23] M. Ciuchini, E. Franco, V. Lubicz, F. Mescia and C. Tarantino, JHEP **0308** (2003) 031 [arXiv:hep-ph/0308029].
- [24] D. Becirevic, V. Gimenez, G. Martinelli, M. Papinutto and J. Reyes, JHEP **0204** (2002) 025 [arXiv:hep-lat/0110091].
- [25] A. Bondar, T. Gershon and P. Krokovny, Phys. Lett. B **624** (2005) 1 [arXiv:hep-ph/0503174].
- [26] K. Abe *et al.*, arXiv:hep-ex/0507065.
- [27] M. Ciuchini *et al.*, JHEP **9810** (1998) 008 [arXiv:hep-ph/9808328].
- [28] D. Becirevic *et al.*, Nucl. Phys. B **634** (2002) 105 [arXiv:hep-ph/0112303].
- [29] See the workshop Lattice QCD: Present and Future, Orsay, April 14-16, 2004,
<http://events.lal.in2p3.fr/conferences/lqcd/friday/lubicz.pdf>,
<http://events.lal.in2p3.fr/conferences/lqcd/friday/sharpe.pdf>,
<http://events.lal.in2p3.fr/conferences/lqcd/friday/giusti2.pdf>.
- [30] LHCb Collaboration, “LHCb technical design report: Reoptimized detector design and performance,” CERN-LHCC-2003-030
- [31] J. Hewett *et al.*, arXiv:hep-ph/0503261.

- [32] D. Bernard et al., “Working Group : CP Violation and Heavy Flavour” for *Journees de perspectives DSM/DAPNIA-IN2P3*,
http://prospective2004.in2p3.fr/textes_definitifs/cp04_final.ps.
- [33] S. Amato *et al.* [LHCb Collaboration], CERN-LHCC-98-4